



Fabrication and characterization of high-strength PVDF/nonwoven fabric electrospun composite membranes for direct contact membrane distillation

Kuiling Li^{a,b}, Jiang Chang^c, Deyin Hou^{a,b,*}, Chunli Ding^d, Jun Wang^b

^aKey Laboratory of Drinking Water Science and Technology, Research Center for Eco-Environmental Sciences, Chinese Academy of Sciences, Beijing 100085, PR China, Tel. +86 10 62917207; Fax: +86 10 62917207; email: dyhou@rcees.ac.cn (D. Hou)

^bState Key Laboratory of Environmental Aquatic Chemistry, Research Center for Eco-Environmental Sciences, Chinese Academy of Sciences, Beijing 100085, PR China

^cLaboratory of Environmental Technology, Institute of Nuclear and New Energy Technology, Tsinghua University, Beijing 100084, PR China

^dSchool of Chemical Engineering and Technology, Hebei University of Technology, Tianjin 300130, PR China

Received 9 April 2017; Accepted 27 September 2017

ABSTRACT

The polyvinylidene fluoride (PVDF) nanofibers composite membranes were fabricated for membrane distillation using polyester nonwoven fabric as a substrate via electrospinning. The influences of nonwoven fabric and electrospinning time on membrane morphology, hydrophobicity, pore size and pore size distribution, porosity, mechanical strength and permeability were evaluated. All the electrospun composite membranes had a three-dimensional bead-fiber interconnected open structure and a rough membrane surface with water contact angle of greater than 140°. The composite membranes obtained high-mechanical strength because of nonwoven fabric substrate, which was important for industrial application. The resultant membranes were tested through direct contact membrane distillation (DCMD) using 3.5 wt% sodium chloride solution as feed, and the highest permeate flux was up to 54.0 kg/m² h at feed temperature of 80°C. The anti-fouling properties of the fabricated membrane were investigated by DCMD experiment with mixed solution including sodium chloride, calcium chloride and humic acid, and the composite membrane presented excellent anti-fouling performance. During sodium chloride solution concentration process, it was demonstrated that the permeability and hydrophobicity of the composite membrane can maintain well after repeated use and rinse. The results suggested the potential of the electrospun PVDF/nonwoven fabric composite membrane for membrane distillation application.

Keywords: Membrane distillation; Hydrophobic surface; Electrospinning; Polyvinylidene fluoride; Nonwoven fabric; Mechanical strength

1. Introduction

Membrane distillation (MD) is a nonisothermal membrane process in which the driving force is the partial pressure gradient across a hydrophobic membrane that directly contacts with the hot feed liquid solution to be treated [1]. MD is investigated worldwide as a low-cost, energy saving alternative to conventional separation processes such as distillation

and reverse osmosis (RO) [2]. Compared with other more popular separation processes, MD is characterized with the distinct advantages of (1) 100% (theoretical) rejection of solute, (2) lower operating temperature than distillation and (3) lower pressure than pressure-driven membrane separation processes such as microfiltration (MF), ultrafiltration (UF) and nanofiltration (NF) [3]. According to the condensation method adopted, MD was developed to direct contact membrane distillation (DCMD), air gap membrane distillation (AGMD), sweeping gas membrane distillation (SGMD) and vacuum membrane distillation (VMD) [4]. At present, MD

* Corresponding author.

has been applied in desalination, juice concentration, crystallization and other industrial areas in laboratory or pilot plant scale [5–9].

The hydrophobic membrane, acting as a physical barrier and providing a liquid–gas interface for mass transfer, plays a crucial role during MD process. The ideal MD membrane should be with high-hydrophobicity, high-porosity, narrow pore size distribution, low-thermal conductivity, and high-physical and chemical stability [10]. The mostly used materials for MD membrane are polytetrafluoroethylene (PTFE), polyvinylidene fluoride (PVDF) and polypropylene (PP) [11]. Compared with other two materials, PVDF is considered promising to prepare MD membrane because of its properties such as greater hydrophobicity and better chemical resistance than PP, and easier manufacture procedure than PTFE. Two main methods are often used to fabricate PVDF membranes, thermally induced phase separation (TIPS) method [12] and nonsolvent induced phase separation (NIPS) method [13]. However, the PVDF membranes prepared by these two methods are usually with low-porosity, wide pore size distribution or poor mechanical performance [14].

Electrospinning is a promising and versatile approach for fabrication of nanometer- or submicrometer-sized fibers under the application of a strong electric field to a polymer or biopolymer liquid solution [15]. Recently, some electrospun nanofibrous membranes have been applied for MD. The membranes fabricated via electrospinning exhibit high-permeate flux and high-salt rejection due to their high-hydrophobicity, high-porosity, low-thickness, and interconnected open structure [16]. The electrospun nanofibers with cylindrical shape feature a rough and re-entrant structure [17], which makes a high-hydrophobic surface and may induce “Cassie-Baxter State” at the interface of water and electrospun nanofibers membrane. Moreover, the thickness of electrospun nanofibers membrane can be controlled through electrospinning time and is generally thinner than that of the membranes fabricated via TIPS and NIPS methods [18], which indicates low-mass transfer resistance and is beneficial to obtain a higher permeate flux.

Previous studies have demonstrated successful fabrication of electrospun nanofibers membranes for MD [19–22]. Feng et al. [23] attempted to use electrospun nanofibers membrane in AGMD to produce potable water from saline water, and demonstrated that the PVDF nanofiber membrane can be used in MD process and the membrane flux was comparable with those obtained by commercial MF membranes. Su et al. [24] fabricated PVDF membrane with the porosity up to 95% by electrospinning, and the permeate flux of the electrospun membrane was significantly higher than that of PTFE commercial membrane. Li et al. [25] obtained a dual-biomimetic polystyrene superhydrophobic electrospun nanofibrous membrane via a one-step electrospinning technique, and the membrane maintained a high and stable permeate water flux compared with typical commercial PVDF MD membranes.

Although the electrospun nanofibers membranes presented satisfying permeability, their mechanical strength should be further improved [26]. After all, the excellent mechanical properties of nanomaterials are essentially in the nanoscale, which do not mean the nanomaterials maintain outstanding mechanical performance in macroscopic

scale. In essence, the electrospun nanofibers membrane can be regarded as a flat-sheet membrane. As for the flat-sheet membrane with a support layer, it will present stronger mechanical strength and can withstand the intense hydraulic impact and flow disturbance, which are very important from an industrial application standpoint.

The present investigation was carried out to fabricate PVDF electrospun composite membrane for MD using polyester (PET) nonwoven fabric as a support. The prepared composite membranes contained a hydrophobic PVDF electrospun nanofibrous separation function layer and a nonwoven fabric support layer, which is expected to obtain both a high-permeate flux and excellent mechanical strength. The composite membranes properties were also tested and characterized in this work.

2. Materials and methods

2.1. Materials

PVDF (FR-904) was obtained from Shanghai 3F New Materials Co., Ltd. (China) and the molecular weight of PVDF is about 1.02×10^6 g/mol. *N,N*-Dimethylformamide (DMF, >99%) was purchased from Shanghai Jingwei Chemical Co., Ltd. (China). Acetone (AR grade, >99.5%) was supplied by Sinopharm Chemical Reagent Co., Ltd. (China). NaCl (anhydrous, >99.5%), CaCl₂ (anhydrous, >97%) and humic acid (HA) were from Beijing Chemical Works (China). The ultra-pure water used in all experiments was produced by a Milli-Q BIOCEL unit (MilliPore, USA) with the resistivity of 18 MΩ cm.

2.2. Membrane preparation

The PVDF resin powders were dried at 100°C under vacuum for 24 h to remove its moisture content before it was used for dope preparation. PVDF powders (12 wt%) were added into the DMF/acetone mixed solvent in which the weight ratio of DMF and acetone was 9:1 and stirred under 50°C until totally solved. Afterwards, the stirring was stopped and the gas bubbles in the polymer solution were released for about 12 h.

To fabricate a flat-sheet composite membrane, a nonwoven fabric was first set on the rotating drum, followed by electrospinning of PVDF fibers on top of the nonwoven fabric. Approximately, 40 mL PVDF polymer solution was loaded into a syringe with a stainless steel 18-gauge needle. The syringe was placed horizontally in a syringe pump (CSP-100C, Shenzhen Carewell Electronics Co., Ltd., China), and a voltage supply (Tong Li Tech. Co., Ltd., China) was connected to the needle tip via an alligator clip. The PVDF fibers were electrospun at an applied voltage of 16 kV. Other parameters as follows: tip-to-collector distance = 15 cm; feed flow rate = 1.5 mL/h; chamber humidity = 30%; chamber temperature = 30°C and drum speed = 150 rpm.

Four PET nonwoven fabrics supplied by BBA Fiberweb (America) are listed in Table 1 and named A, B, C, and D, respectively. The composite membranes using different nonwoven fabric support spun for 12 h were labeled as M-A-12, M-B-12, M-C-12 and M-D-12, respectively, and another two membranes spun on the nonwoven fabric B for 18 and 24 h were named M-B-18 and M-B-24, respectively. After electrospinning,

the fabricated composite membranes were dried in air at room temperature to remove the residual solvents.

2.3. Membrane morphology study

The morphology of membrane was investigated with a field emission scanning electron microscopy (FESEM; Hitachi SU-70, Japan). Membrane samples were frozen in liquid nitrogen, fractured to obtain fragments, and sputtered with platinum using a HITACHI E-1010 Ion Sputtering device for FESEM observation.

2.4. Contact angle measurement

The wettability of membrane surface was exhibited by gauges of contact angle of water droplet with the OCA20 Video-Based Contact Angle Meter (DataPhysics Instruments Ltd., Germany). Water droplet of 0.8 μL was carefully dropped onto the membrane surface through a syringe under ambient temperature and the in-air sessile drop contact angle with water was determined 10 s after water droplet dropping on the membrane surface. The contact angle of the membrane surface with water was obtained by measuring five different positions of each sample.

2.5. Porosity, pore size and pore size distribution

The term porosity is expressed as the volume ratio of pores and total membrane. For calculating the porosity, the membrane sample with a certain area was wetted first. The liquid used to wet membrane sample was supported by IB-FT GmbH (Germany) named Porefil and its surface tension and density were 16 dyn/cm and 1.87 g/mL, respectively. The whole porosity of the composite membrane ε_T and the porosity of the nanofibers layer ε_m were determined by gravimetric method and calculated by the following equations:

$$\varepsilon_T = \frac{m_1 - m_2}{\rho_L \cdot A \cdot l} \quad (1)$$

$$\varepsilon_m = 1 - \frac{m_2 - m_3}{\rho_P \cdot A \cdot l_m} \quad (2)$$

where m_1 , m_2 and m_3 were the weight of wet composite membrane sample, the weight of dry composite membrane sample, the weight of dry nonwoven fabric sample, respectively. A was the area of membrane sample, l and l_m were the thickness of the composite membrane and its nanofibers layer, respectively. ρ_L and ρ_P were the density of Porefil and PVDF, respectively.

Table 1
Parameters of the nonwoven fabric support materials

| Nonwoven fabric | T (fabric thickness, mm) | W (area weight, g/m ²) | W/T (g/cm ³) |
|-----------------|----------------------------|--------------------------------------|----------------------------|
| A | 0.15 \pm 0.003 | 100 \pm 0.6 | 0.67 |
| B | 0.12 \pm 0.002 | 80 \pm 0.5 | 0.67 |
| C | 0.22 \pm 0.003 | 140 \pm 0.6 | 0.64 |
| D | 0.30 \pm 0.004 | 100 \pm 0.6 | 0.33 |

The pore size distributions of the fabricated composite membranes were investigated by using a Capillary Flow Porometer (CFP; Porolux 1000, IB-FT GmbH). The membranes were fully wetted with the Porefil, and then the measurement was carried out following the procedure described in Khayet and Matsuura [27]. The bubble point and mean pore size were determined with the aid of the computer software coupled to CFP.

2.6. Mechanical properties test

The fabricated membrane mechanical properties were measured with an Instron tensiometer (Instron 5565-5kN, Instron Corporation, USA) at room temperature. The flat-sheet membrane sample with an initial length of 8.0 cm and a width of 3.0 cm was clamped at both ends and pulled in tension at a constant elongation rate of 10 mm/min along the length, and five specimens were tested for each membrane sample.

2.7. Desalination experiment

DCMD experiments were carried out with 3.5 wt% sodium chloride solution as feed to evaluate the permeability of the fabricated composite membranes. The schematic representation of DCMD setup is shown in Fig. 1. The membrane module was a plate and frame consisting of two chambers, one for the feed and the other for distillate. The membrane with effective area of $7.47 \times 10^{-3} \text{ m}^2$ was tightly clamped between the two chambers. Both chambers had a thickness of 1.0 mm and there were 10 flow paths with width of 7.0 mm for each chamber. The feed and the distillate were concurrently circulated in membrane module with the help of two magnetic pumps (MP-215R, Shanghai Seisun Bumps, China) and the flow rates of these two fluids kept constant at 70 L/h (about 0.28 m/s). The temperature difference between feed and the distillate side ranged from 20°C to 60°C, and the temperature of the distillation was maintained constant at 20°C. The salinity of the distillate was calculated from the measured conductivity based on a pre-established calibration curve. The permeate flux J (kg/m² h) was calculated by the following equation:

$$J = \frac{m}{A \cdot \Delta t} \quad (3)$$

where m was the mass of produced water in kg, A was the effective contact area of feed and membrane in m² and Δt was the operation time in h.

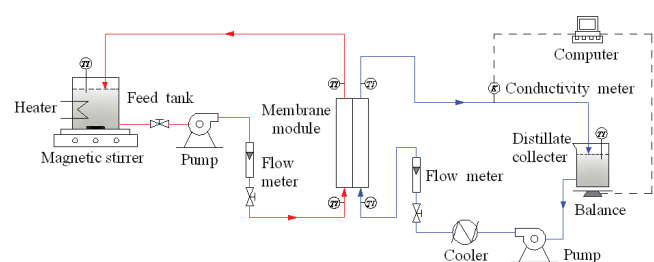


Fig. 1. Schematic diagram of the experimental DCMD setup.

2.8. Membrane anti-fouling evaluation

The anti-fouling properties of the fabricated membrane were tested by carrying out DCMD experiment with high concentrations of NaCl (100 g/L), HA (20 mg/L) and CaCl₂ (20 mM) in the feed solution. The feed side and the permeate side were kept at a constant temperature of 50°C and 20°C, respectively. To investigate the stability of the fabricated membrane and the influence of inorganic salt crystals on MD performance during desalination process, the NaCl aqueous solution (3.5 wt%) was continuously concentrated at the hot side until the permeate flux decrease by 50%, then the membrane was rinsed 5 min with deionized water. After being dried in oven with the temperature of 50°C, the rinsed membrane was employed to a new test cycle. After each cycle, the contact angle of the rinsed membrane was measured to investigate its resistance to wetting during MD.

3. Results and discussions

3.1. Nonwoven fabric substrates structure and permeability

The scanning electron microscopy (SEM) images of the four PET nonwoven fabrics are shown in Fig. 2. It can be found that the nonwoven fabrics A and B were denser than C and D, while the nonwoven fabric A was about 30 μm thicker than B. The nonwoven fabric D was the thickest and loosest in these four nonwoven fabrics. It has been reported that a too denser nonwoven fabric substrate was unfavorable to permeability of the resultant composite membranes fabricated via NIPS method [28]. In this study, the result of gas permeate flux test of the nonwoven fabrics can be found in Fig. 3, which showed that the fabric D with the loosest construction had an outstanding gas permeate flux. The densest fabrics A and B had the lowest gas permeate fluxes

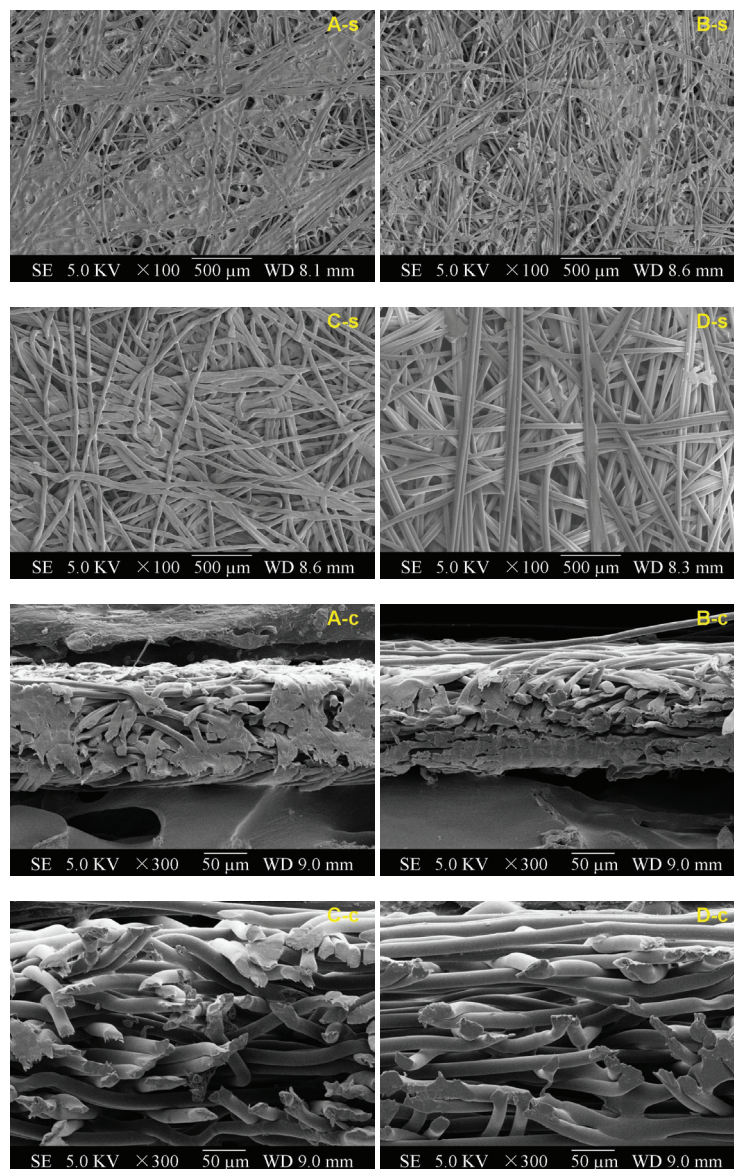


Fig. 2. SEM images of the surface and cross-section of the nonwoven fabrics. A-s, B-s, C-s and D-s are the surface images, and A-c, B-c, C-c and D-c are the cross-section images.

during the four PET nonwoven fabrics, and the thinner nonwoven fabric B had a slightly higher gas permeate flux compared with the nonwoven fabric A. The less difference of gas permeate flux between the nonwoven fabrics A and B may be owing to the less thickness difference and the similar structure.

3.2. Electrospun nanofibers membrane morphology

The surface and cross-section SEM images of the electrospun nanofibers membranes are shown in Fig. 4. It can be observed that the electrospun fibrous layers combined very well with the nonwoven fabrics. All the membranes surfaces present a bead-fiber interconnected structure and the beads randomly distribute in the fibrous network. The higher magnification pictures show a “three-dimensional (3D)” nanofiber interconnected open structure. The 3D bead-fiber interconnected open structure endowed the electrospun composite membrane with a rough membrane surface, which may make a Cassie-Baxter state [29] occur at the interface of water and membrane due to the multilevel re-entrant structure in the membrane surface. Therefore, the 3D bead-fiber

interconnected open structure would characterize the electrospun nanofibers membranes with good hydrophobicity and facilitate the MD performance.

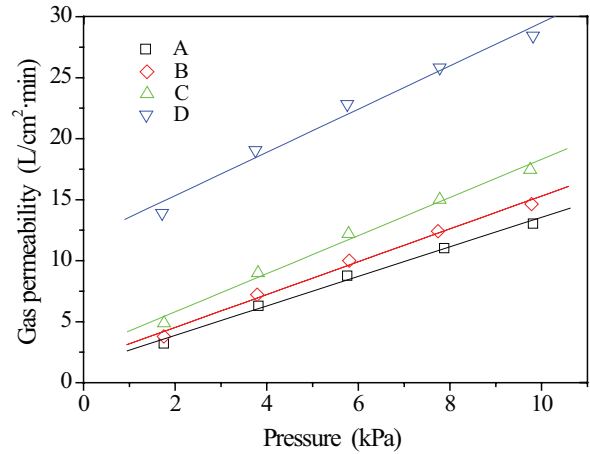


Fig. 3. Gas permeate flux of the nonwoven fabrics.

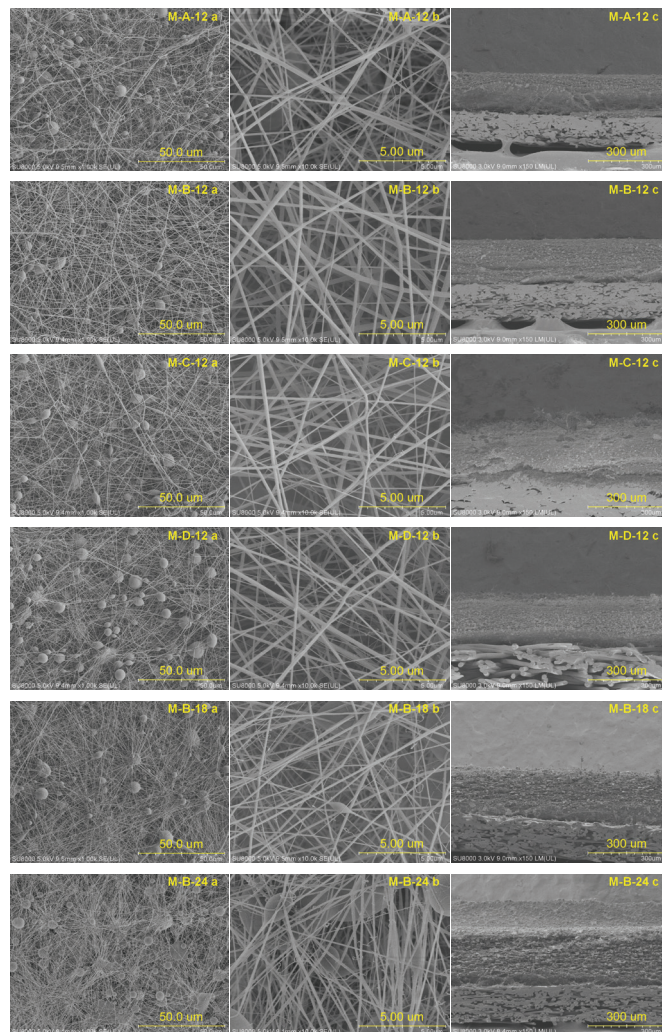


Fig. 4. SEM images of the surface and cross-section of the electrospun composite membranes.

The diameter distribution of the electrospun fibers can be obtained with the aid of the computer software coupled to SEM. According to the statistical results as presented in Fig. 5, M-C-12 had the greatest mean fiber diameter, about 145 ± 13 nm. The mean fiber diameters of M-A-12, M-B-12, M-D-12, M-B-18 and M-B-24 were about 108 ± 20 nm, 127 ± 15 nm, 130 ± 10 nm, 110 ± 15 nm and 103 ± 17 nm, respectively. The statistical results also revealed that the size distribution of the nanofibers of M-C-12 was the broadest and the nanofibers diameter ranged from 50 to 230 nm. The size distribution of the nanofibers of M-B-12 was the narrowest and the nanofibers diameter ranged from 45 to 185 nm. For the composite membranes electrospun 12 h, the mean fiber diameter of M-A-12 was the smallest which might induce a lower thickness and poor mechanical strength of the nanofibers layer. In the surface of M-D-12, more beads can be clearly observed compared with other composite membranes.

The composite membranes M-B-12, M-B-18 and M-B-24 were fabricated using same nonwoven fabrics as substrate, however, the electrospinning time increasing led to a decrease

of the mean diameter of nanofibers, which may be attributed to the change of tip-to-collector distance. The longer time of spinning increased membrane thickness, which meant that the rotating drum diameter increased and the tip-to-collector distance reduced. The decrease of tip-to-collector distance induced electric field intensity enhancement which would improve the volatilization rate of the mixed solvent. In addition, the increase of the rotating drum diameter with electrospinning time increasing made a larger drawing ratio. The higher solvent volatilization speed and larger drawing ratio resulted in thinner nanofibers formation in the electrospun composite membrane surface.

3.3. Nanofibers membrane structural attributes

A hydrophobic surface is necessary for the membrane used in MD to prevent liquid from permeating through the membrane. The in-air sessile drop contact angles with water for the fabricated membranes are presented in Fig. 6, which indicates that all the membrane surfaces constructed

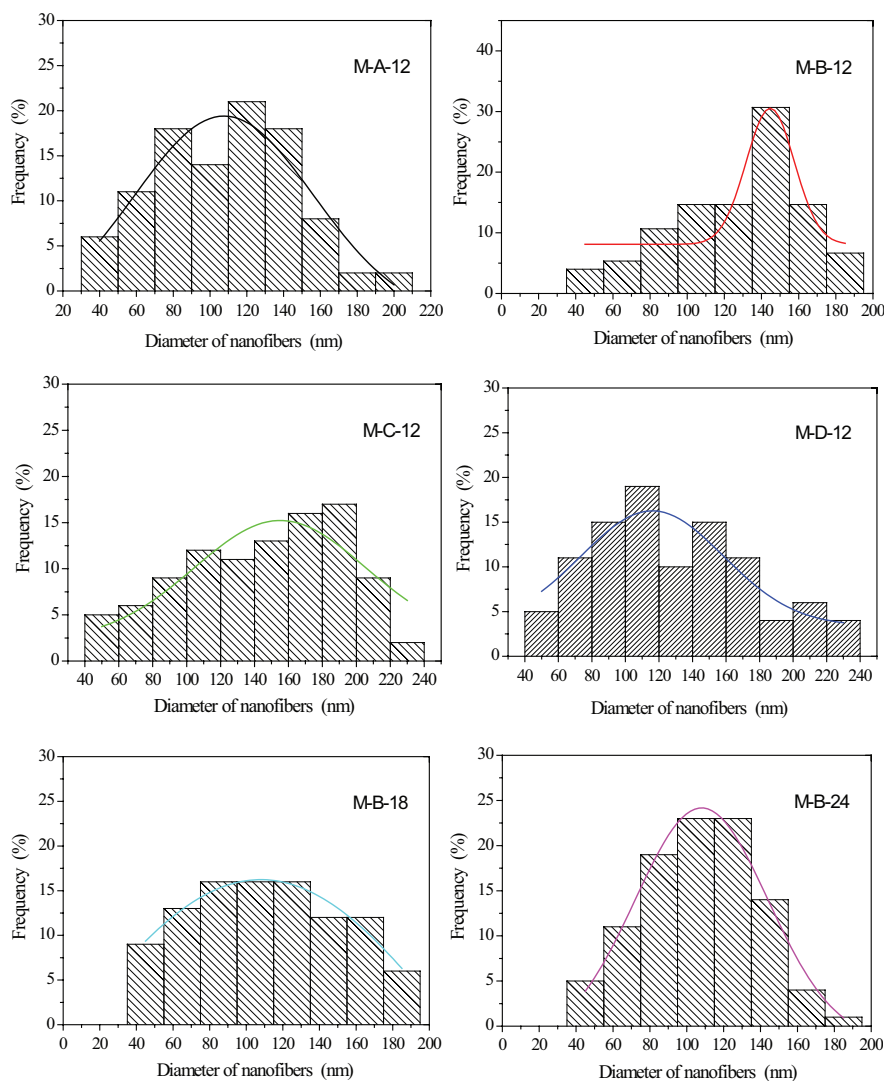


Fig. 5. The diameter distribution of the electrospun nanofibers.

of electrospun nanofibers are hydrophobic. For hydrophobic materials, a rougher surface is helpful to reach greater hydrophobicity or superhydrophobicity by achieving Cassie-Baxter state. The electrospun nanofibers with cylindrical shape featured a rougher and re-entrant structure, which rendered the hydrophobic surface with higher water repellency. In Fig. 6, it can be observed that all the contact angles for the electrospun composite membranes were greater than 140° . In the surface of M-D-12, there were many beads interweaved with the nanofibers, which introduced hierarchical roughness and made the membrane surface near to superhydrophobic that was defined as contact angle greater than 150° [30]. Compared the composite membranes M-B-18 and M-B-24 with M-B-12, it can be found that the electrospinning time increasing was beneficial to membrane surface hydrophobicity in some extent. This result may be explained by the fact that the 3D bead-fiber interconnected open structure and hydrophobic materials were distinct with maintenance of air in the surface as well as within the bulk of the fibrous layer of the composite membranes, which can continuously provide a new water–air–material interface as water contacts the membrane [31].

The thickness, porosity, pore size and liquid entry pressure of water (LEPw) of the electrospun composite membranes are listed in Table 2. The total porosity of the composite membranes ranged from 62.1% to 79.8%, and the porosity of the electrospun fibrous layer ranged from 87.5% to 92.6%,

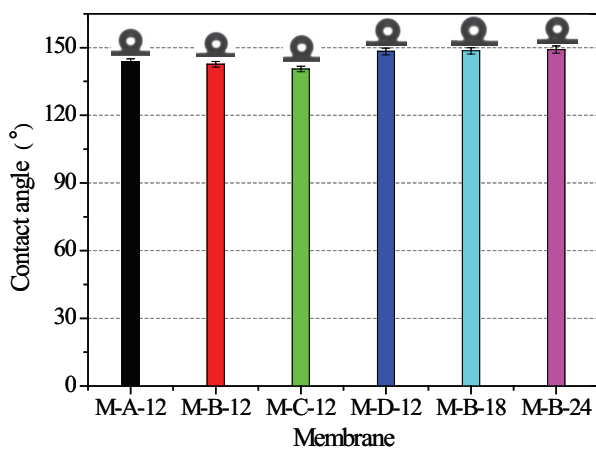


Fig. 6. The contact angles of the electrospun nanofibers membranes.

Table 2
Structural attributes of the electrospun composite membranes

| Membranes | Total thickness (μm) | Nanofibers layer thickness (μm) | Total porosity (%) | Nanofibers layer porosity (%) | Mean pore size (μm) | LEPw (10^3 Pa) |
|-----------|-----------------------------------|--|--------------------|-------------------------------|----------------------------------|-------------------|
| M-A-12 | 269 ± 12 | 115 ± 8 | 69.7 ± 1.2 | 91.2 ± 1.3 | 1.62 ± 0.16 | 45.1 ± 0.4 |
| M-B-12 | 225 ± 15 | 108 ± 7 | 71.0 ± 1.1 | 89.4 ± 0.9 | 1.78 ± 0.13 | 44.5 ± 0.3 |
| M-C-12 | 331 ± 11 | 112 ± 7 | 62.1 ± 1.2 | 91.0 ± 1.2 | 1.94 ± 0.15 | 42.8 ± 0.2 |
| M-D-12 | 396 ± 17 | 98 ± 12 | 73.5 ± 1.2 | 88.3 ± 1.1 | 2.02 ± 0.11 | 43.6 ± 0.3 |
| M-B-18 | 312 ± 9 | 186 ± 9 | 72.3 ± 1.1 | 92.6 ± 1.2 | 1.42 ± 0.08 | 71.3 ± 0.5 |
| M-B-24 | 470 ± 14 | 320 ± 8 | 79.8 ± 1.2 | 93.4 ± 0.9 | 1.25 ± 0.13 | 77.9 ± 0.6 |

which indicated that the electrospun fibrous network can endow the hydrophobic separation functional layer with higher porosity due to the interconnected open structure. The total porosity of M-C-12 was much lower than that of others because of the highest area weight of the nonwoven fabric C. There was no significant difference on porosity of the electrospun fibrous layers for all the composite membranes, while the electrospinning time increasing can improve membrane porosity due to the fibrous layer thickness increase. The fibrous layers of the resultant composite membranes had an interconnected open structure without “blind pores”, and higher porosity meant the membrane had more pore channels for vapor diffusion hence leading to a higher permeate flux. Additionally, high-porosity membrane with more void space can also increase the thermal resistance of the membrane and therefore decreases the heat conductivity across the membrane [32].

The pore size distribution of the electrospun composite membranes can be seen in Fig. 7. The mean pore sizes of the four composite membranes M-A-12, M-B-12, M-C-12 and M-D-12 were 1.62, 1.78, 1.94 and $2.02 \mu\text{m}$, respectively, it can be found that the substrate can influence membrane pore size and the composite membrane using the loosest nonwoven fabric D as substrate obtained the largest mean pore diameter. Comparing the three composite membranes spun on the nonwoven fabric B, we can clearly found that with the increase of electrospinning time, the mean pore size decreased from $1.78 \mu\text{m}$ (M-B-12) to $1.25 \mu\text{m}$ (M-B-24), and the pore size distribution was narrowed. The LEPw values can be obtained using the method described by Smolders and Franken [33]. In Table 2, it can be found that the LEPw values of the composite membranes electrospun 12 h were less than 50 kPa, and the electrospinning time increasing can improve the LEPw value to more than 70 kPa. The membrane with small mean pore size and narrow pore size distribution are considered to have a better maintenance of salt rejection and a less chance of being wetted. However, with the increase of spinning time, the thickness increased and mean pore size decreased, which may induce lower permeate flux during MD practice.

3.4. Nanofibers membrane mechanical properties

In order to investigate mechanical properties of the fabricated membranes, the pure PVDF nanofibers membrane electrospun 12 h and PVDF/nonwoven fabric electrospun composite membranes were all stretched. The stress–strain

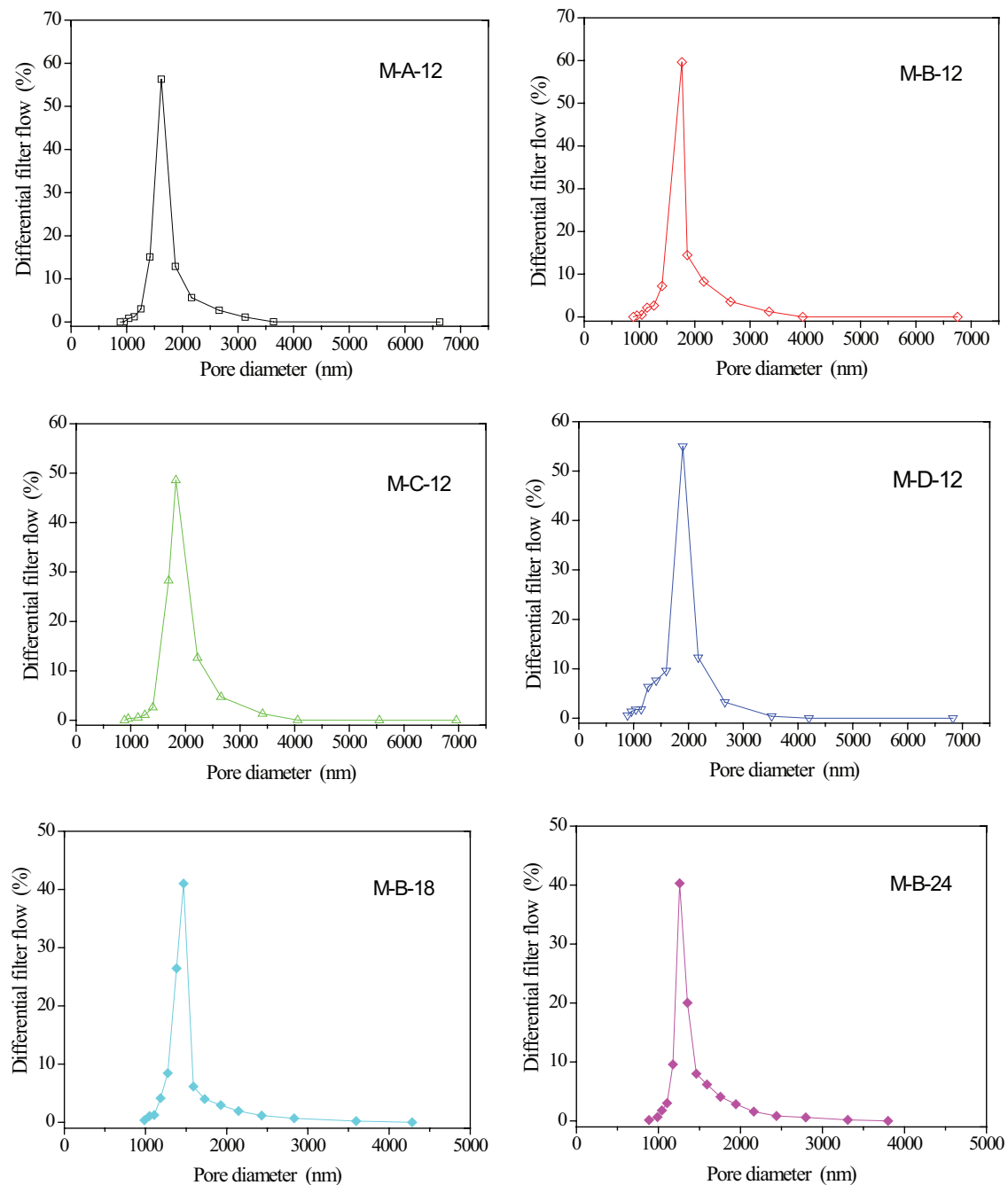


Fig. 7. Pore size distribution of the electrospun nanofibers membranes.

curves of the membranes are shown in Fig. 8 and the corresponding experimental data are listed in Table 3.

All the composite membranes exhibited pronounced rigidity behavior compared with the pure electrospun PVDF nanofibers membrane. However, except M-D-12, the ductility of all the composite membranes decreased significantly, which vitally depend on the properties of the nonwoven fabrics, and this result also indicated that the substrate material should be taken into account to enhance the composite mechanical strength. The less strain of the composite membranes electrospun on nonwoven fabrics of A, B and C was mainly because of the broken nonwoven fabric substrates. These three nonwoven

fabric substrates broke in prior of the electrospun nanofibers layer and led to the break of the composite membranes. For the composite membranes electrospun on the nonwoven fabric B, the electrospinning time increasing had negligible impact on the membrane stress, which also indicated that the nonwoven fabric substrate, on the other hand, can determine the mechanical properties of the composite membranes.

Although the stress at break of M-D-12 was about 13.0 MPa, the load at break of this composite membrane was about 154.0 N, which meant that this composite membrane actually had a strong stretching strength and the relative low-stress can be attributed to the highest membrane thickness

compared with other three composite membranes electrospun 12 h. The strain of M-D-12 was the highest during all the electrospun composite membranes, which demonstrated that the nonwoven fabric D itself had a good ductility. In Table 3, it can also be seen that the mechanical performance of the composite membrane M-D-12 was superior to the pure electrospun PVDF nanofibers membrane. The MD process is usually operated in normal atmospheric pressure or below it and the requirement of hydrophobic membrane mechanical properties is lower than that of the membrane used for pressure-driven membrane process such as MF and UF, however, excellent mechanical properties can offer hydrophobic membrane great potential to be applied in MD industrialization process considering the hydraulic impact and flow disturbance.

3.5. Membrane distillation performance

The permeate flux of composite membranes electrospun on different nonwoven fabric substrate at different feed temperature is presented in Fig. 9. All the membranes showed an increasing trend of permeate flux with the increase of feed temperature due to the enhanced vapor pressure at the feed–membrane interface. Among the four composite nanofibers membranes electrospun on different nonwoven fabric for 12 h, the M-B-12 membrane showed the best permeability. The highest permeate flux was up to $54.0 \text{ kg/m}^2 \text{ h}$ at the feed temperature of 80°C for the M-B-12 membrane. The good

permeability of the electrospun composite membrane can be mainly attributed to the special membrane structure. Compared with conventional hydrophobic membranes fabricated through phase inversion, the membrane prepared by electrospinning had an interconnected open structure with high-porosity, which indicated that there were more through channels for vapor diffusion and the mass transfer resistance was effectively reduced, therefore, the electrospun composite membrane obtained a high-permeate flux during MD process. However, it should be noted that the nonwoven fabric substrate may counteract the advantage of the electrospun nanofibers layer. The M-D-12 membrane, for example, had the largest mean pore size and the highest total porosity among the four composite nanofibers membranes electrospun 12 h, but its permeate flux was lower than that of the M-B-12, and this result can be attributed to the highest thickness of the nonwoven fabric D which increased the mass transfer resistance compared with nonwoven fabric B.

The influence of electrospinning time on membrane permeability is illustrated in Fig. 10. It can be found that the increase of electrospinning time induced a low-permeate flux. The longer is the electrospinning time, the thicker will be the membrane. The electrospinning time increasing also reduced mean pore size of the composite membranes. In addition, the increase of thickness enlarged the mass transfer distance, and improved pores tortuosity of the composite membrane. As a result, the mass transfer resistance was improved and the permeate flux declined. During the membrane permeability test process, the conductivity of the distillate from all the electrospun composite membranes was less than $10.0 \mu\text{S/cm}$, which indicated that the salt rejection achieved 99.99% for the composite membranes.

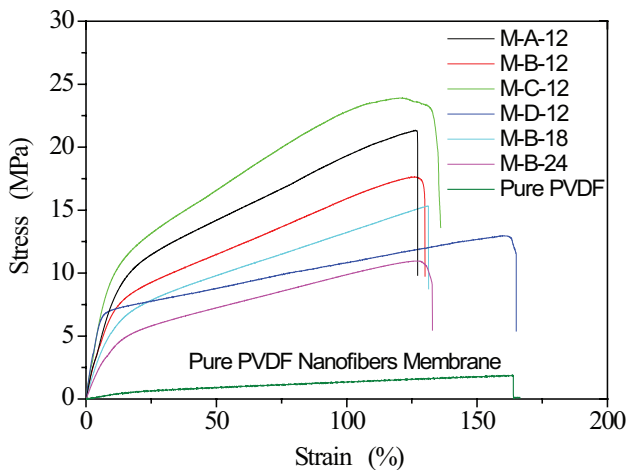


Fig. 8. Stress–strain curves of the fabricated membranes.

3.6. Membrane anti-fouling evaluation

To investigate the anti-fouling performance of the fabricated composite membrane, DCMD experiment with a 120 h period was carried out using the mixed solution including NaCl (100 g/L), CaCl_2 (20 mM) and HA (20 mg/L) as the feed, the M-B-12 membrane with the highest permeate flux among the composite membranes was selected to be tested. Fig. 11 shows the variations of permeation flux and permeate conductivity with operating time in the test process. In terms of the permeation flux, it can be noted that the permeate flux had a negligible decline at the first 45 h, and then started to decrease. However, at the end of the experiment, the permeate flux declined only about 25%. In the case of the

Table 3
Mechanical properties of the electrospun composite membranes

| Membrane code | Stretching strain at break (%) | Stress at break (MPa) | Load at break (N) | Elastic modulus (MPa) |
|---------------|--------------------------------|-----------------------|-------------------|-----------------------|
| Pure PVDF | 164.39 ± 3.57 | 1.86 ± 1.71 | 6.43 ± 0.79 | 7.35 ± 1.08 |
| M-A-12 | 127.53 ± 2.45 | 21.32 ± 2.03 | 172.05 ± 3.60 | 138.71 ± 5.16 |
| M-B-12 | 130.02 ± 2.30 | 17.63 ± 0.95 | 129.00 ± 5.15 | 165.37 ± 3.35 |
| M-C-12 | 136.16 ± 3.55 | 23.90 ± 1.58 | 237.32 ± 8.62 | 220.68 ± 4.63 |
| M-D-12 | 164.98 ± 2.37 | 12.96 ± 1.92 | 153.96 ± 4.59 | 153.45 ± 5.36 |
| M-B-18 | 131.45 ± 3.62 | 15.33 ± 1.85 | 143.68 ± 4.16 | 181.72 ± 3.87 |
| M-B-24 | 132.85 ± 3.08 | 10.96 ± 2.53 | 154.53 ± 6.35 | 207.79 ± 4.64 |

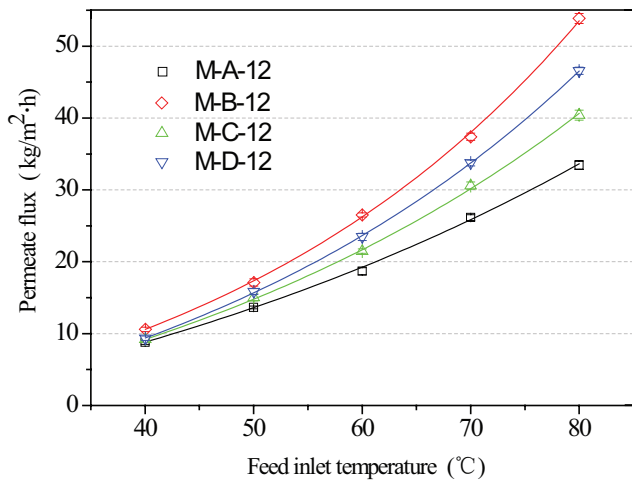


Fig. 9. The permeate flux of the nanofiber membranes electrospun on different nonwoven fabric substrate. NaCl aqueous solution (3.5 wt%) was used as the feed. The flow rate at feed and permeate side were 70 L/h. The distillate temperature was 20°C.

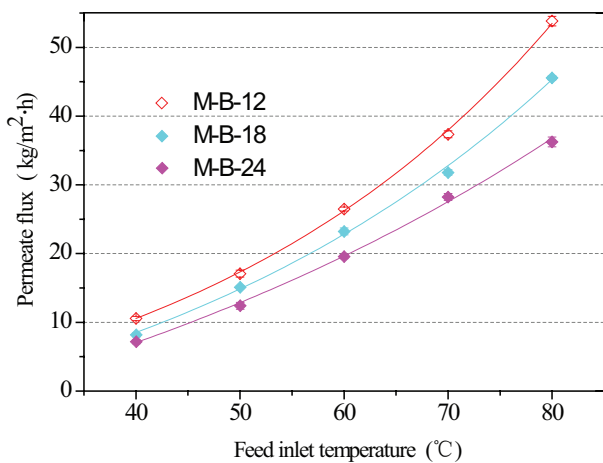


Fig. 10. The permeate flux of the nanofiber membranes electrospun on the nonwoven fabric B. NaCl aqueous solution (3.5 wt%) was used as the feed. The flow rate at feed and permeate side were 70 L/h. The distillate temperature was 20°C.

conductivity, it can be observed that the permeate conductivity maintained below 10 $\mu\text{S}/\text{cm}$ during the whole experiment process, which indicated that the composite membrane pores could not be wetted easily. In the SEM image of the fouled membrane as shown in Fig. 12, it can be found that the foulants scattered on membrane surface and covered part of membrane surface.

Interestingly, no foulant was observed in the inner pores of the composite membrane. This is mainly because of the 3D bead-fiber structure of the composite membrane. The hydrophobic fibrous membrane surface made it was difficult for the foulants to adsorb and accumulate on the membrane surface. Besides, the electrospun fibers close to membrane surface acted a role of a filter, which prevented the foulants infiltrating into the deeper of the overlapping fibers. Therefore, although the accumulated foulants on the membrane surface caused the mass transfer resistance to increase and declined

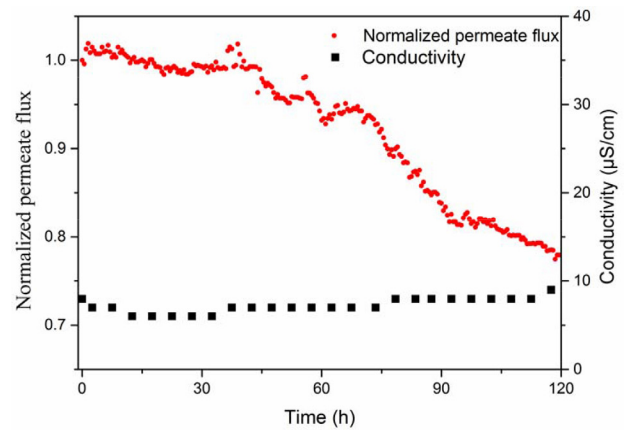


Fig. 11. Permeate flux and permeate conductivity varied with operating time for the M-B-12 composite membrane. The flow rate at feed and permeate side were 70 L/h. The feed temperature was 50°C. The distillate temperature was 20°C. The mixed solution including NaCl (100 g/L), CaCl_2 (20 mM) and HA (20 mg/L) was used as the feed.

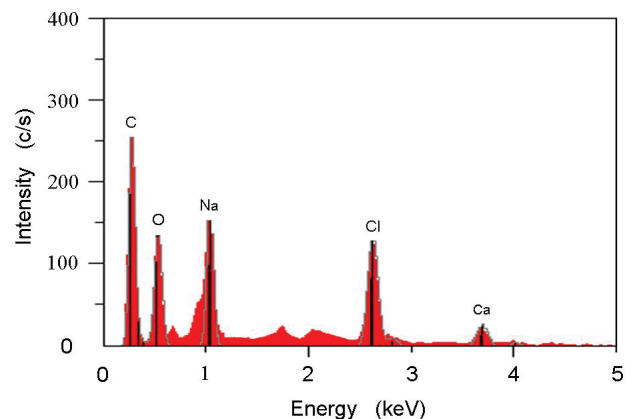
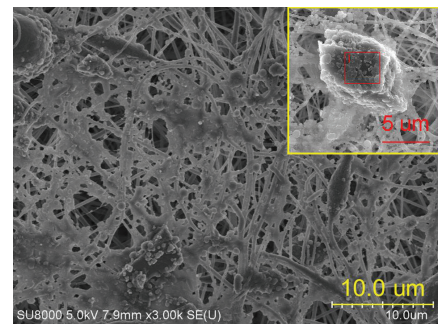


Fig. 12. SEM image of the fouled membrane and elemental analysis of the foulants.

the permeation flux, the fibrous network beneath the surface still kept dry and hydrophobic. As a result, the permeate conductivity can maintain below 10 $\mu\text{S}/\text{cm}$ during the whole experiment process.

The stability of the fabricated composite membrane and the influence of inorganic salt crystals on MD performance during desalination process were also investigated through

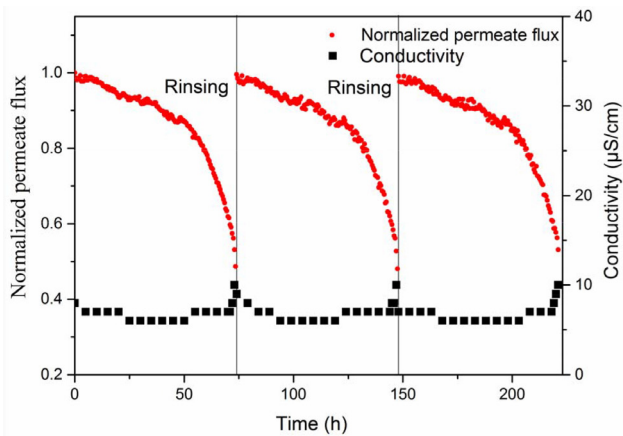


Fig. 13. Permeate flux and permeate conductivity varied with operating time for the M-B-12 composite membrane during NaCl solution concentration through MD. The flow rate at feed and permeate side were 70 L/h. The feed temperature was 50°C. The distillate temperature was 20°C. NaCl aqueous solution (3.5 wt%) was used as the feed to be concentrated in each cycle.

concentration of the NaCl aqueous solution. During the concentration process, the MD experiment stopped when the permeate flux declined 50%, and the composite membrane was rinsed with deionized water. Undoubtedly, the rinsed membrane must be completely dry when it was employed on next concentration experiment. The change of permeate flux and permeate conductivity can be found in Fig. 13. In each cycle, the flux decreased steadily at the first 45 h and then declined sharply until to 50%. Although the permeate conductivity increased to about 10 $\mu\text{S}/\text{cm}$ in the last few hours in each cycle, it kept stable in most of the time. The salt rejection of the fabricated composite membrane can maintain as high as 99.99% during the salt solution concentration process, which indicated a high-resistance of the composite membrane against inorganic salt crystals.

With the NaCl concentration increasing, the concentration polarization adjacent membrane surface became more and more intense, the fibers near membrane surface served as crystal nucleuses in some extent, and most of the salt crystals formed at the cross of fibers or coated the fibers except for a few large-size crystals scattering on membrane surface as shown in Fig. 14. On the other hand, similar to the case of membrane fouling by HA, the 3D interconnected open structure of the composite membrane can also prevent wetting and crystallizing into deeper fibrous layer. After each rinse, the permeate flux was totally recovered, which also indicated that the salt crystals only deposited near the fibrous membrane surface and can be easily washed away. The test results of the membrane surface hydrophobicity before and after using in MD concentration are presented in Fig. 15. It can be found that the contact angle of the membrane surface stabilized in the range of 140°–143°, which demonstrated that the membrane hydrophobicity can also maintain well after repeated use and rinse. These results showed that the fabricated composite membrane exhibited satisfying performance stability, which indicated the composite membrane may be of great potential to be utilized in the MD process.

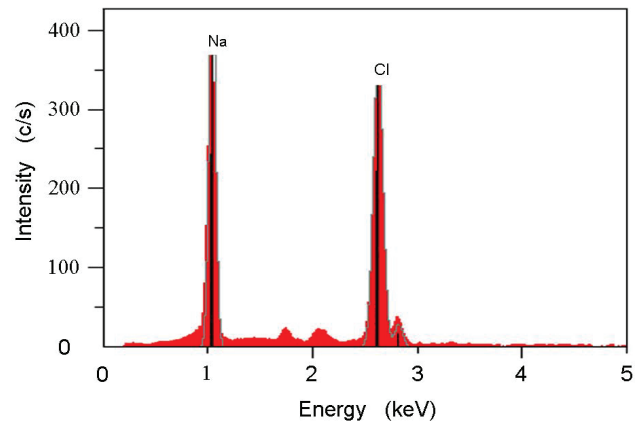
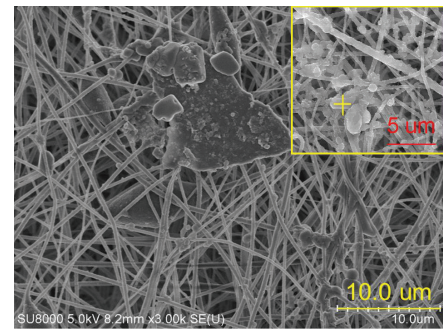


Fig. 14. SEM image of the membrane after using in MD concentration and elemental analysis of the salt crystals deposited on membrane surface.

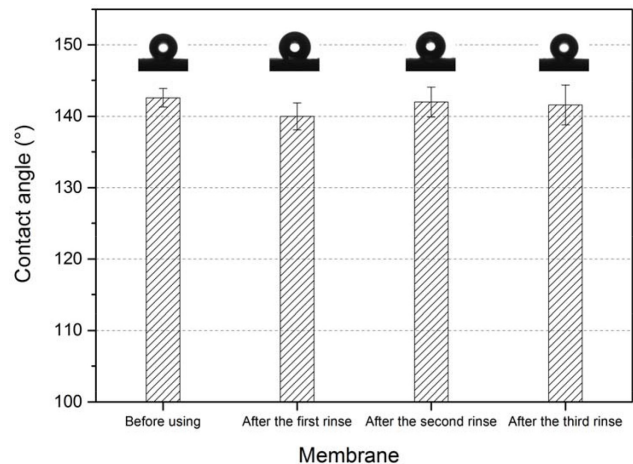


Fig. 15. The contact angle of the M-B-12 composite membrane before and after using in MD concentration.

4. Conclusion

In this work, the PVDF nanofibers composite membranes were fabricated for MD using PET nonwoven fabric as a substrate via electrospinning.

The electrospun PVDF nanofibers layer presented a 3D bead-fiber interconnected open structure, which endowed the composite membranes with a rough membrane surface.

Meanwhile, the membrane surface had a multilevel re-entrant structure and all the contact angles of the membranes were greater than 140° and even very near to 150°.

The electrospun composite membranes with appropriate pore size and narrow pore size distribution, high-porosity, excellent hydrophobicity and good permeability fulfilled the requirements of MD application. Compared with the pure electrospun PVDF nanofibers membrane, the composite membranes exhibited stronger mechanical properties, which was important from an industrial application standpoint.

The fabricated membranes were tested through DCMD using 3.5 wt% NaCl solution as feed, and the highest permeate flux was up to 54.0 kg/m² h at the feed temperature of 80°C and the rejection of NaCl maintained 99.99%. In addition, the anti-fouling properties of the fabricated membrane were investigated with mixed solution including sodium chloride, calcium chloride and humic acid, and the electrospun membrane presented excellent anti-fouling performance. During sodium chloride solution concentration process, the permeability and hydrophobicity of the composite membrane maintained well after repeated use and rinse. It is believed that the fabricated PVDF/nonwoven fabric electrospun composite membrane may be of great potential to be utilized in the MD process.

Acknowledgments

Financial supports provided by the National Natural Science Foundation of China (grant numbers 51478454 and 51678555) and the special fund of State Key Joint Laboratory of Environment Simulation and Pollution Control (grant number 16L02ESPC) are gratefully acknowledged.

References

- [1] M. Khayet, Membranes and theoretical modeling of membrane distillation: a review, *Adv. Colloid Interface Sci.*, 164 (2011) 56–88.
- [2] A. Alkhudhiri, N. Darwish, N. Hilal, Membrane distillation: a comprehensive review, *Desalination*, 287 (2012) 2–18.
- [3] S. Al-Obaidani, E. Curcio, F. Macedonio, G.D. Profio, H. Al-Hinai, E. Drioli, Potential of membrane distillation in seawater desalination: thermal efficiency, sensitivity study and cost estimation, *J. Membr. Sci.*, 323 (2008) 85–98.
- [4] E. El-Zanati, K.M. El-Khatib, Integrated membrane-based desalination system, *Desalination*, 205 (2007) 15–25.
- [5] K. Gethard, O. Sae-Khow, S. Mitra, Water desalination using carbon-nanotube-enhanced membrane distillation, *ACS Appl. Mater. Interfaces*, 3 (2011) 110–114.
- [6] K. Bélafi-Bakó, B. Koroknai, Enhanced water flux in fruit juice concentration: coupled operation of osmotic evaporation and membrane distillation, *J. Membr. Sci.*, 269 (2006) 187–193.
- [7] X. Jia, E. Curcio, S.A. Obaidani, G.D. Profio, E. Fontananova, E. Drioli, Membrane distillation-crystallization of seawater reverse osmosis brines, *Sep. Purif. Technol.*, 71 (2010) 76–82.
- [8] Q. Ge, P. Wang, C. Wan, T.S. Chung, Polyelectrolyte-promoted forward osmosis-membrane distillation (FO-MD) hybrid process for dye wastewater treatment, *Environ. Sci. Technol.*, 46 (2012) 6236–6243.
- [9] G. Lewandowicz, W. Białas, B. Marczewski, D. Szymanowska, Application of membrane distillation for ethanol recovery during fuel ethanol production, *J. Membr. Sci.*, 375 (2011) 212–219.
- [10] M.S. El-Bourawi, Z.W. Ding, R.Y. Ma, M. Khayet, A framework for better understanding membrane distillation separation process, *J. Membr. Sci.*, 285 (2006) 4–29.
- [11] P. Wang, T.S. Chung, Recent advances in membrane distillation processes: membrane development, configuration design and application exploring, *J. Membr. Sci.*, 474 (2015) 39–56.
- [12] L. Lin, H. Geng, Y. An, P. Li, H. Chang, Preparation and properties of PVDF hollow fiber membrane for desalination using air gap membrane distillation, *Desalination*, 367 (2015) 145–153.
- [13] C.Y. Kuo, H.N. Lin, H.A. Tsai, D.M. Wang, J.Y. Lai, Fabrication of a high hydrophobic PVDF membrane via nonsolvent induced phase separation, *Desalination*, 233 (2008) 40–47.
- [14] D. Hou, J. Wang, X. Sun, Z. Ji, Z. Luan, Preparation and properties of PVDF composite hollow fiber membranes for desalination through direct contact membrane distillation, *J. Membr. Sci.*, 405–406 (2012) 185–200.
- [15] H.G. Wang, S. Yuan, D.L. Ma, X.B. Zhang, J.M. Yan, Electrospun materials for lithium and sodium rechargeable batteries: from structure evolution to electrochemical performance, *Energy Environ. Sci.*, 8 (2015) 1660–1681.
- [16] L.D. Tijing, J.S. Choi, S. Lee, S.H. Kim, H.K. Shon, Recent progress of membrane distillation using electrospun nanofibrous membrane, *J. Membr. Sci.*, 453 (2014) 435–462.
- [17] J. Lee, C. Boo, W.H. Ryu, A.D. Taylor, M. Elimelech, Development of omniphobic desalination membranes using a charged electrospun nanofiber scaffold, *ACS Appl. Mater. Interfaces*, 8 (2016) 11154–11161.
- [18] L. Lin, M. Danilczuk, S. Schlick, Electron spin resonance study of chemical reactions and crossover processes in a fuel cell: effect of membrane thickness, *J. Power Sources*, 233 (2013) 98–103.
- [19] Y. Liao, R. Wang, M. Tian, C. Qiu, A.G. Fane, Fabrication of polyvinylidene fluoride (PVDF) nanofiber membranes by electro-spinning for direct contact membrane distillation, *J. Membr. Sci.*, 425–426 (2013) 30–39.
- [20] M. Essalhi, M. Khayet, Self-sustained webs of polyvinylidene fluoride electrospun nano-fibers: effects of polymer concentration and desalination by direct contact membrane distillation, *J. Membr. Sci.*, 454 (2014) 133–143.
- [21] J.A. Prince, G. Singh, D. Rana, T. Matsuura, V. Anbharasi, T.S. Shanmugasundaram, Preparation and characterization of highly hydrophobic poly(vinylidene fluoride)-clay nanocomposite nanofiber membranes (PVDF-clay NMs) for desalination using direct contact membrane distillation, *J. Membr. Sci.*, 397–398 (2012) 80–86.
- [22] B.S. Lalia, E. Guillen-Burrieza, H.A. Arafat, R. Hashaikheh, Fabrication and characterization of polyvinylidene fluoride-co-hexafluoropropylene (PVDF-HFP) electrospun membranes for direct contact membrane distillation, *J. Membr. Sci.*, 428 (2013) 104–115.
- [23] C. Feng, K.C. Khulbe, T. Matsuura, R. Gopal, S. Kaur, S. Ramakrishna, M. Khayet, Production of drinking water from saline water by air-gap membrane distillation using polyvinylidene fluoride nanofiber membrane, *J. Membr. Sci.*, 311 (2008) 1–6.
- [24] C.I. Su, J.H. Shih, M.S. Huang, C.M. Wang, W.C. Shih, Y.S. Liu, A study of hydrophobic electrospun membrane applied in seawater desalination by membrane distillation, *Fibers Polym.*, 13 (2012) 698–702.
- [25] X. Li, C. Wang, Y. Yang, X. Wang, M. Zhu, B.S. Hsiao, Dual-biomimetic superhydrophobic electrospun polystyrene nanofibrous membranes for membrane distillation, *ACS Appl. Mater. Interfaces*, 6 (2014) 2431–2438.
- [26] M. Essalhi, M. Khayet, Self-sustained webs of polyvinylidene fluoride electrospun nanofibers at different electrospinning times: 1. Desalination by direct contact membrane distillation, *J. Membr. Sci.*, 433 (2013) 167–179.
- [27] M. Khayet, T. Matsuura, Preparation and characterization of polyvinylidene fluoride membranes for membrane distillation, *Ind. Eng. Chem. Res.*, 40 (2001) 5710–5718.
- [28] D. Hou, G. Dai, J. Wang, H. Fan, L. Zhang, Z. Luan, Preparation and characterization of PVDF/nonwoven fabric flat-sheet composite membranes for desalination through direct contact membrane distillation, *Sep. Purif. Technol.*, 101 (2012) 1–10.

- [29] T. Darmanin, F. Guittard, Recent advances in the potential applications of bioinspired superhydrophobic materials, *J. Mater. Chem. A*, 2 (2014) 16319–16359.
- [30] K.Y. Law, Water-surface interactions and definitions for hydrophilicity, hydrophobicity and superhydrophobicity, *Pure Appl. Chem.*, 87 (2015) 759–765.
- [31] Y. Liao, C.H. Loh, R. Wang, A.G. Fane, Electrospun superhydrophobic membranes with unique structures for membrane distillation, *ACS Appl. Mater. Interfaces*, 6 (2014) 16035–16048.
- [32] J. Phattaranawik, R. Jiraratananon, A.G. Fane, Heat transport and membrane distillation coefficients in direct contact membrane distillation, *J. Membr. Sci.*, 212 (2003) 177–193.
- [33] K. Smolders, A.C.M. Franken, Terminology for membrane distillation, *Desalination*, 72 (1989) 249–262.